Pradeep K. Khosla*
Takeo Kanade**
Department of Electrical and Computer Engineering
The Robotics Institute
Carnegie Mellon University
Pittsburgh, Pennsylvania 15213

Experimental Evaluation of Nonlinear Feedback and Feedforward Control Schemes for Manipulators

Abstract

The manipulator trajectory tracking control problem revolves around computing the torques to be applied to achieve accurate tracking. This problem has been extensively studied in simulations, but real-time results have been lacking in the robotics literature. In this paper, we present the experimental results of the real-time performance of model-based control algorithms. We compare the computed-torque control scheme with the feedforward dynamics compensation scheme. The feedforward scheme compensates for the manipulator dynamics in the feedforward path, whereas the computed-torque scheme uses the dynamics in the feedback loop for linearization and decoupling. The parameters in the dynamics model for the computed-torque and feedforward schemes were estimated by using an identification algorithm. Our experiments underscore the importance of including the off-diagonal terms of the manipulator inertia matrix in the torque computation. This observation is further supported by our analysis of the dynamics equations. The manipulator control schemes have been implemented on the CMU DD arm II with a sampling period of 2 ms.

* Assistant Professor of Electrical and Computer Engineering.

** Professor of Computer Science and Robotics.

Research based upon work supported by National Science Foundation Grant ECS-8320364.

The International Journal of Robotics Research,
Vol. 7, No. 1, February 1988,

1. Introduction

The manipulator control problem revolves around the computation of the joint torques required to track the desired joint position, velocity, and acceleration trajectories. This problem has been studied extensively in the robotics literature and many schemes have been proposed (Bejczy 1974, Brady et al. 1982, Freund 1982, Gilbert and Ha 1984, Horowitz and Tomizuka 1980, Liegois et al. 1980, Raibert and Horn 1978, Seraji 1986, Slotine 1985, Tourassis 1985). Although many simulation results have been presented, real-time implementation and performance evaluation of model-based control schemes on actual manipulators has not been performed. The main reasons for this are that (1) the high gear ratios and the dominant friction effects in commercial geared manipulators make them unsuitable for real-time performance evaluation; (2) the computational requirements of the Newton-Euler algorithm are still beyond the reach of commercially available microprocessors (Kanade et al. 1984) for high sample-rate control; and (3) it has been difficult to obtain an accurate model because research in this area has been lacking.

One of the goals of the CMU directdrive arm II (Schmitz et al. 1985) project is to demonstrate the effect of full dynamics compensation on the real-time trajectory performance tracking of manipulators by overcoming the above-mentioned difficulties. To overcome the hurdle posed by the computational requirements, we have customized the Newton-Euler algorithm and achieved a computational cycle of 1.2 ms. This permits us to implement control algorithms at

high sampling rates of up to 830 Hz. We have also proposed numerical (Khosla 1986) and symbolic algorithms (Khosla and Kanade 1986, Neuman and Khosla 1985) to estimate the dynamic parameters of a manipulator. Further, we have implemented the identification algorithm to experimentally estimate the dynamic parameters of the six-degrees-of-freedom CMU direct-drive arm 11. The estimated parameters were used to implement and evaluate the performance of both the computed-torque and feedforward control schemes.

The above developments have allowed us to implement and evaluate the real-time performance of advanced manipulator control schemes. The experimental results of the real-time implementation and evaluation of model-based control schemes were presented recently, wherein the performance of the computed-torque and the independent joint control schemes was compared (Khosla and Kanade 1986). We have also experimentally evaluated the effect of the control sampling rate on the performance of model-based schemes (Khosla 1987).

In this paper, we compare the computed-torque scheme with the feedforward dynamics compensation scheme. Other researchers have also addressed this problem and evaluated the real-time performance of the model-based schemes (Leahy et al. 1986, An 1986). Both the computed-torque and the feedforward schemes use the full dynamics model of the manipulator but in different paths of the control loop: The feedforward scheme compensates for the manipulator dynamics in the feedforward path, and the computed-torque scheme uses the dynamics in the feedback loop. By injecting the torque as a feedforward signal, the feedforward scheme effectively linearizes the manipulator system about a given trajectory. However, it does not achieve *exact decoupling.* In contrast, the computed-torque scheme, by utilizing the dynamics model in the feedback loop, achieves both linearization and decoupling. The control schemes have been implemented on the CMU DD arm II with a sampling period of 2 ms (or a control sampling rate of 500 Hz).

This paper is organized as follows. The manipulator control schemes that have been implemented and evaluated are presented in Section 2. The design of the controller gain matrices is outlined in Section 3. In Section 4, we delineate and analyze the results of our real-time implementation. In Section 5, we draw our conclusions.

2. Manipulator Control Techniques

The dynamics of a manipulator are described by a set of highly nonlinear and coupled differential equations. The complete dynamic model of an N-degrees-of-freedom manipulator is

$$\tau = \mathbf{D}(\theta)\ddot{\theta} + \mathbf{h}(\theta, \dot{\theta}) + \mathbf{g}(\theta), \qquad (1)$$

where τ is the N-vector of the actuating torques; $\mathbf{D}(\theta)$ is the N x N positiondependent manipulator inertia matrix; $\mathbf{h}(\theta, \dot{\theta})$ is the N-vector of Coriolis and centrifugal torques; $\mathbf{g}(\theta)$ is the N-vector of gravitational torques; and $\ddot{\theta}$, $\dot{\theta}$, and θ are N-vectors of the joint accelerations, velocities, and positions, respectively.

We have implemented and compared the performance of the computed-torque and feedforward compensation control schemes. In order to evaluate the effect of approximating the positiondependent inertia matrix $\mathbf{D}(\theta)$ by a constant diagonal inertia matrix $\mathbf{J}$, we have also implemented the reduced feedforward compensation scheme. In the sequel, K_p and K_v are the constant and diagonal position and velocity feedback gain matrices, respectively; θ and θ_d are the measured and reference joint position vectors, respectively; and the dot denotes the derivative with respect to time.

Computed-Torque Control Scheme (CT)

This scheme, depicted in Fig. 1, utilizes nonlinear feedback to decouple the manipulator. The control torque τ is computed by the inverse dynamics equation in (1), using the commanded acceleration instead of the measured acceleration $\ddot{\theta}$, as

$$\tau = \tilde{\mathbf{D}}(\theta)[\mathbf{K}_p(\theta_d - \theta) + \mathbf{K}_v(\dot{\theta}_d - \dot{\theta}) + \ddot{\theta}_d] + \tilde{\mathbf{h}}(\theta, \dot{\theta}) + \tilde{\mathbf{g}}(\theta), \qquad (2)$$

where ~ indicates that the estimated values of the dynamics parameters are used in the computation.

Fig. 1. Block diagram of computed-torque control scheme.

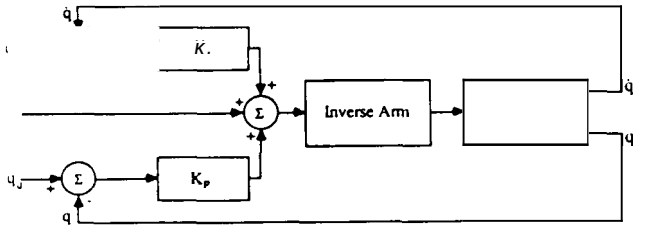

Fig. 2. Block diagram of feedforward compensation control scheme.

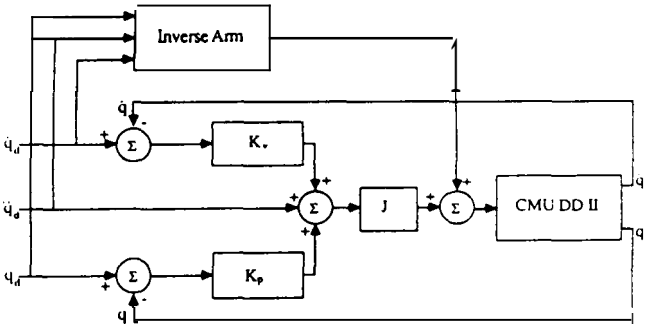

Feedforward Dynamics Compensation Scheme (FED)

If the dynamics model of a manipulator is ***exact,*** then the application of joint torques computed from (1) by using the reference trajectory will accomplish trajectory tracking. In practice, however, the presence of modeling errors creates the need for a feedback controller to compensate for the small deviations in trajectory tracking. The feedforward dynamics compensation technique, depicted in Fig. 2, is based on the premise that the ***gross*** torque for trajectory tracking is provided by using the inverse dynamics model in (1) in the feedforward path. This control signal is then augmented with the signal derived from linear independent joint controllers, which are assumed to correct for the small deviations in trajectory tracking. The control torque τ is therefore

$$\tau = \tilde{\mathbf{D}}(\theta_d)\ddot{\theta}_d + \tilde{\mathbf{h}}(\theta_d, \dot{\theta}_d) + \tilde{\mathbf{g}}(\theta_d) + \mathbf{J}[\mathbf{K}_p(\theta_d - \theta) + \mathbf{K}_v(\dot{\theta}_d - \dot{\theta})], \quad (3)$$

where the first three terms are the feedforward compensation torque, the last term is the torque due to the feedback controller, and **J** is the N **X** N diagonal matrix of link inertias at a typical position.

Reduced Feedforward Compensation Scheme (RFED)

The reduced feedforward compensation scheme, depicted in Fig. 3, has been implemented to demonstrate the effect of approximating the positiondependent inertia matrix by a constant diagonal matrix. The control torque is computed by substituting the constant diagonal inertia matrix J instead ***of*** $\mathbf{D}(\theta_d)$ in the first term in (3). Thus the torque applied to the joints **at** each sampling instant is

$$\tau = \mathbf{J}[\mathbf{K}_p(\theta_d - \theta) + \mathbf{K}_v(\dot{\theta}_d - \dot{\theta}) + \ddot{\theta}_d] + \tilde{\mathbf{h}}(\theta_d, \dot{\theta}_d) + \tilde{\mathbf{g}}(\theta_d), \quad (4)$$

where τ is the N-vector of applied control torques and J is the N **X** ***N*** diagonal matrix of link inertias at a typical position.

The application of the above control laws is based on the assumption that the joint drive system is **a** torque-controlled device. To ensure that the above assumption is satisfied, we have identified the characteristics of the joint drive systems. The CMU DD arm **II** has very little friction and is driven by brushless dc torque motors with amplifiers that control motor current rather than voltage or speed.

We conducted the open-loop small-signal frequency-response analysis and identified the continuous-time transfer function of each joint. Since our sampling period of 2 ms is about 10 times smaller than the dominant mechanical time constant of the system, we assume that the effects of sampling are not evident in the input-output response of the system. This assumption is indeed supported by the experimental results. The identified transfer functions are depicted in Table 1.

3. Controller Design

The performance of the control schemes presented in the previous section can **be** compared only if the same criteria are used for design of the controller gain matrices. Fortunately, this **is** possible because the gain matrices **K,** and $\mathbf{K}_v$ are the same for all three control schemes in this paper. Khosla and Kanade (1986) give a detailed procedure for choosing these gain matrices and establishing an equivalence between the gains of

Fig. 3. Block diagram of independent joint control scheme.

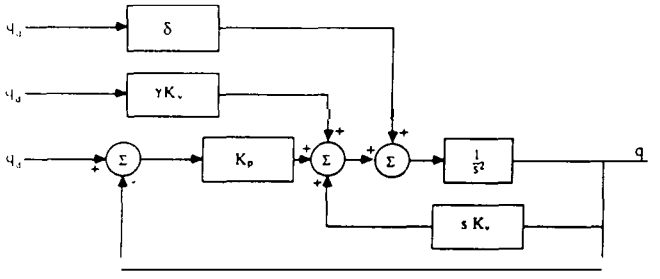

the nonlinear computed-torque scheme and the linear independent joint control scheme. For expository convenience, we outline the criteria for the selection of the gain matrices for the computed-torque scheme. In our experiments, we used these gain values for implementing and evaluating the performance of the RFED and FED schemes also.

Table 1. Transfer Functions and Gains of Individual Links

Joint (j)	*Transfer Function* $(1/J_j s^2)$	k_{pj}	k_{vj}
1	$\frac{1}{12.3s^2}$	40.0	12.6
2	$\frac{1}{2s2}$	58.0	15.2
3	$\frac{1}{0.25s^2}$	400.0	40.0
4	$\frac{1}{0.007s^2}$	2800.0	106.0
5	$\frac{1}{0.006s^2}$	1200.0	69.3
6	$\frac{1}{0.0003s^2}$	3000.0	110.0

3.1. Design of Gain Matrices for Computed-Torque Scheme

The basic idea behind the computed-torque scheme is to achieve dynamic decoupling of all the joints using nonlinear feedback. If the dynamic model of the manipulator is described by (1) and the applied control torque is computed according to (2), then the following closed-loop system is obtained:

$$\ddot{\theta} = \mathbf{u}_i - [\tilde{\mathbf{D}}]^{-1}\{[\mathbf{D} - \tilde{\mathbf{D}}]\ddot{\theta} + [\mathbf{h} - \tilde{\mathbf{h}}] + [\mathbf{g} - \tilde{\mathbf{g}}]\},$$

where $\mathbf{u}_i$ is the commanded acceleration signal, and the functional dependencies on θ and $\dot{\theta}$ have been omitted for the sake of clarity. If the dynamics are modeled exactly, that is, $\tilde{\mathbf{D}} = \mathbf{D}$, $\tilde{\mathbf{h}} = \mathbf{h}$, and $\tilde{\mathbf{g}} = \mathbf{g}$, then the decoupled closed loop system is

$$\ddot{\theta} = \mathbf{u}_i. \tag{5}$$

The commanded acceleration signal is typically computed as (Khosla and Kanade 1986)

$$\mathbf{u}_i = \mathbf{K}_p(\theta_d - \theta) + \mathbf{K}_v(\dot{\theta}_d - \dot{\theta}) + \ddot{\theta}_d. \tag{6}$$

Substituting (6) in (5) gives the following closed-loop characteristic equation for all the joints:

$$s^2 + k_{vj}s + k_{pj} = 0, \tag{7}$$

where k_{vj} and k_{pj} are the velocity and position gains for the jth joint.

Since we do not want any joint to overshoot the commanded position or alternately the response to be critically damped, our choice of the matrices $\mathbf{K}_v$ and $\mathbf{K}_p$ must be such that their elements satisfy the condition:

$$k_{vj} = 2\sqrt{k_{pj}} \qquad \text{for } j = 1, \ldots, 6. \tag{8}$$

Besides, in order to achieve a high disturbance rejection ratio or high stiffness, we must also choose the position gain matrix $\mathbf{K}_p$ as large as possible, which gives a large $\mathbf{K}_v$.

In practice, however, the choice of the velocity gain $\mathbf{K}_v$ is limited by the noise present in the velocity measurement. The dependence of the velocity gain on the noise may be a serious drawback if the velocity is obtained by numerically differentiating the position measurements. In our system, we use 16-bit resolvers to obtain the position measurements of each joint. The

Fig. 4. Schematic diagram of 3-dof DD arm II.

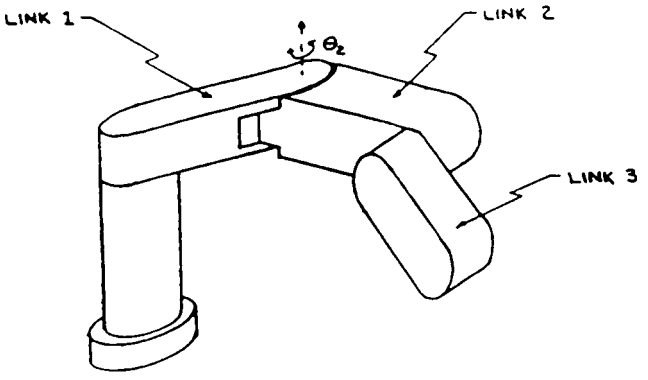

velocity is obtained by using tachometers that are incorporated in the resolver-todigital (R/D) converters boards. Since the **R/D** boards compute the velocity by integrating a signal that is proportional to the acceleration, the velocity measurements are ***relatively*** noise free.

We determined the upper limit of the velocity gain experimentally. We set the position gain to zero and increased the velocity gain of each joint until the unmodeled high-frequency dynamics of the system were excited by the noise introduced in the velocity measurement. This value of $\mathbf{K}_v$ represents the maximum allowable velocity gain. We chose **80%** of the maximum velocity gain in order to obtain as high a value of the position gain as possible and still be well within the stability limits with respect to the unmodeled high-frequency dynamics. The elements of the position gain matrix $\mathbf{K}_p$ were computed to satisfy the critical damping condition in **(8)** and to achieve the maximum disturbance rejection ratio. The elements of the velocity and position gain matrices used in the implementation of the control schemes are listed in Table 1.

4. Experiments and Results

4.1. Trajectory Selection and Evaluation Criteria

Since the DD arm II is a highly nonlinear and coupled system, it is impossible to characterize its behavior from a particular class of inputs, unlike linear systems for which a specific input (such as a unit step or a ramp) can be used to design and evaluate the controllers. Thus an important constituent of the experi-

Fig. 5. Desired trajectories for joint 1.

Fig. 6. Desired trajectories *for joint 2.*

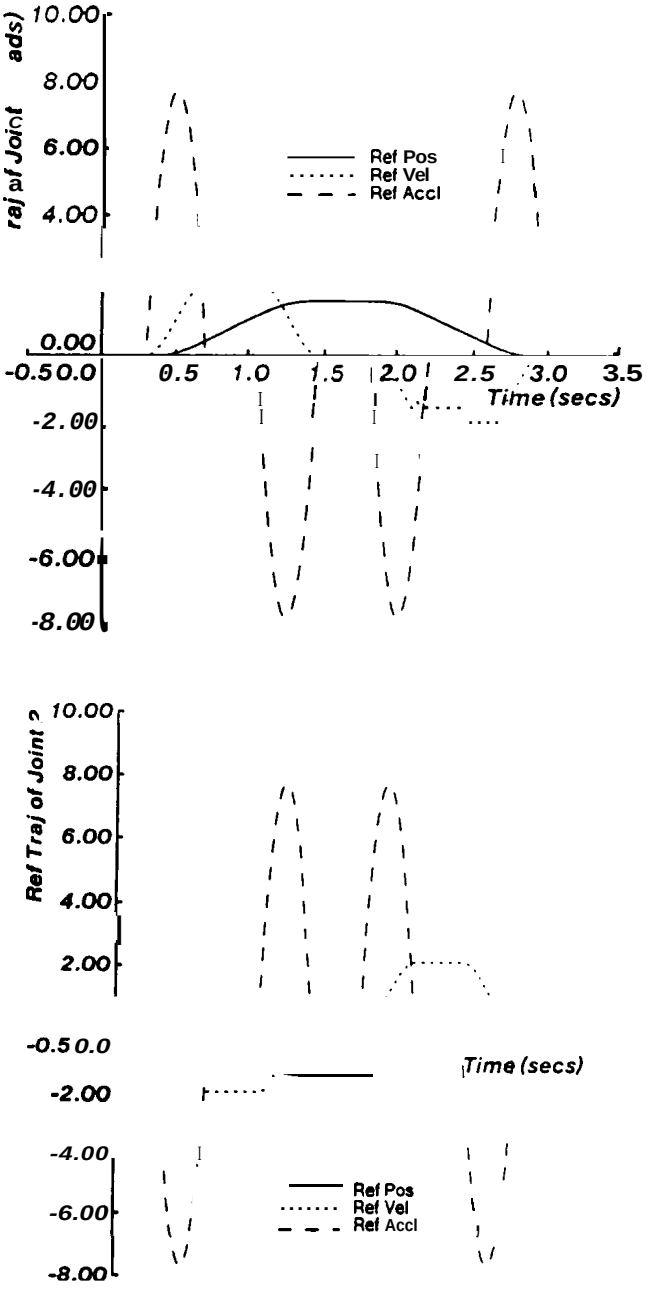

Table 2. Maximum Tracking Errors for T1

	CT		RFED		FED	
Joint No.	Pos Error (rad)	Vel Error (rad/s)	Pos Error (rad)	Vel Error (rad/s)	Pos Error (rad)	Vel Error (rad/s)
1	0.082	0.35	0.03	0.20	0.036	0.40
2	0.11	0.55	0.18	0.88	0.13	0.58
3	0.008	0.008	0.026	0.23	0.056	0.2

mental evaluation of robot control schemes is the choice of a class of inputs for the robot. Khosla (1986) gives the criteria for selecting the joint trajectories.

For evaluating the performance of robot control schemes, we used the dynamic tracking accuracy. This is defined as the maximum position and velocity tracking error along a specified trajectory.

4.2. Real-Time Results

We have implemented the control schemes CT, FED, and RFED, presented in Section 2, and evaluated their real-time performance on the six-degrees-of-freedom CMU DD arm II. Because of lack of space, we present our results for a simple but illustrative trajectory used to evaluate the above-mentioned control schemes.

The trajectory is chosen to be simple and relatively slow but capable of providing insight into the effect of dynamics compensation. In this trajectory only joints 1 and 2 move while all the other joints are commanded to hold their zero positions and can be envisioned from the schematic diagram in Fig. 4. Joint 1 is commanded to start from its zero position and to reach the position of 1.5 rad in 0.75 s. It remains at this position for an interval of 0.75 s, after which it is required to return to its home position in 0.75 s. Similarly, joint 2 is commanded to start from its zero position and to reach the position of -1.5 rad in 0.75 s. It remains at this position for an interval of 0.75 s, after which it is required to return to its home position in 0.75 s. The points of discontinuity, in the trajectory, were joined by a fifth-order polynomial to maintain the continuity of position, velocity, and acceleration along the three segments. The desired position, velocity, and acceleration trajectories for joints 1 and 2 are depicted in Figs. 5 and 6, respectively. The absolute value of the maximum velocity and acceleration to be attained by joints 1 and 2 are 2 rad/s and 7.5 rad/s^2, respectively.

The position and velocity tracking curves for schemes CT, RFED, and FED are depicted in Figs. 7–10. The corresponding position and velocity tracking errors in the three schemes for each joint are shown in Figs. 11–16. To give an idea of the relative performances, the maximum position and velocity tracking errors of each joint are depicted in Table 2. For the sake of brevity we have not included the graphs or tabulated the values of the errors of the last three wrist joints.

To help us interpret the experimental results, we outline the dynamic equations for the first three degrees of freedom of the CMU DD arm II:

$$\tau_1 = d_{11}\ddot{\theta}_1 + d_{12}\ddot{\theta}_2 + d_{13}\ddot{\theta}_3 + h_{133}\dot{\theta}_3^2 + h_{122}\dot{\theta}_2^2 + 2h_{123}\dot{\theta}_2\dot{\theta}_3 + 2h_{113}\dot{\theta}_1\dot{\theta}_3 + 2h_{112}\dot{\theta}_1\dot{\theta}_2, \quad (9)$$

$$\tau_2 = d_{21}\ddot{\theta}_1 + d_{22}\ddot{\theta}_2 + d_{23}\ddot{\theta}_3 + h_{233}\dot{\theta}_3^2 + h_{223}\dot{\theta}_2\dot{\theta}_3 + 2h_{213}\dot{\theta}_1\dot{\theta}_3 - h_{211}\dot{\theta}_1^2, \quad (10)$$

$$\tau_3 = d_{31}\ddot{\theta}_1 + d_{32}\ddot{\theta}_2 + d_{33}\ddot{\theta}_3 - h_{322}\dot{\theta}_2^2 - 2h_{312}\dot{\theta}_1\dot{\theta}_2 - h_{311}\dot{\theta}_1^2 + g_3. \quad (11)$$

The coefficients d_{ij}, h_{ijk}, and g_i are functions of the joint position vector θ and are given by Khosla and Kanade (1985).

The applied torque signals for the three schemes are shown in Figs. 17–19. Further, decomposition of the applied torques in CT into the inertial, the centrifugal,

Fig. 7. Position tracking of joint 1.

Fig. 8. Position tracking of joint 2.

Fig. 9. Velocity tracking of joint 1.

Fig. 10. Velocity tracking of joint 2.

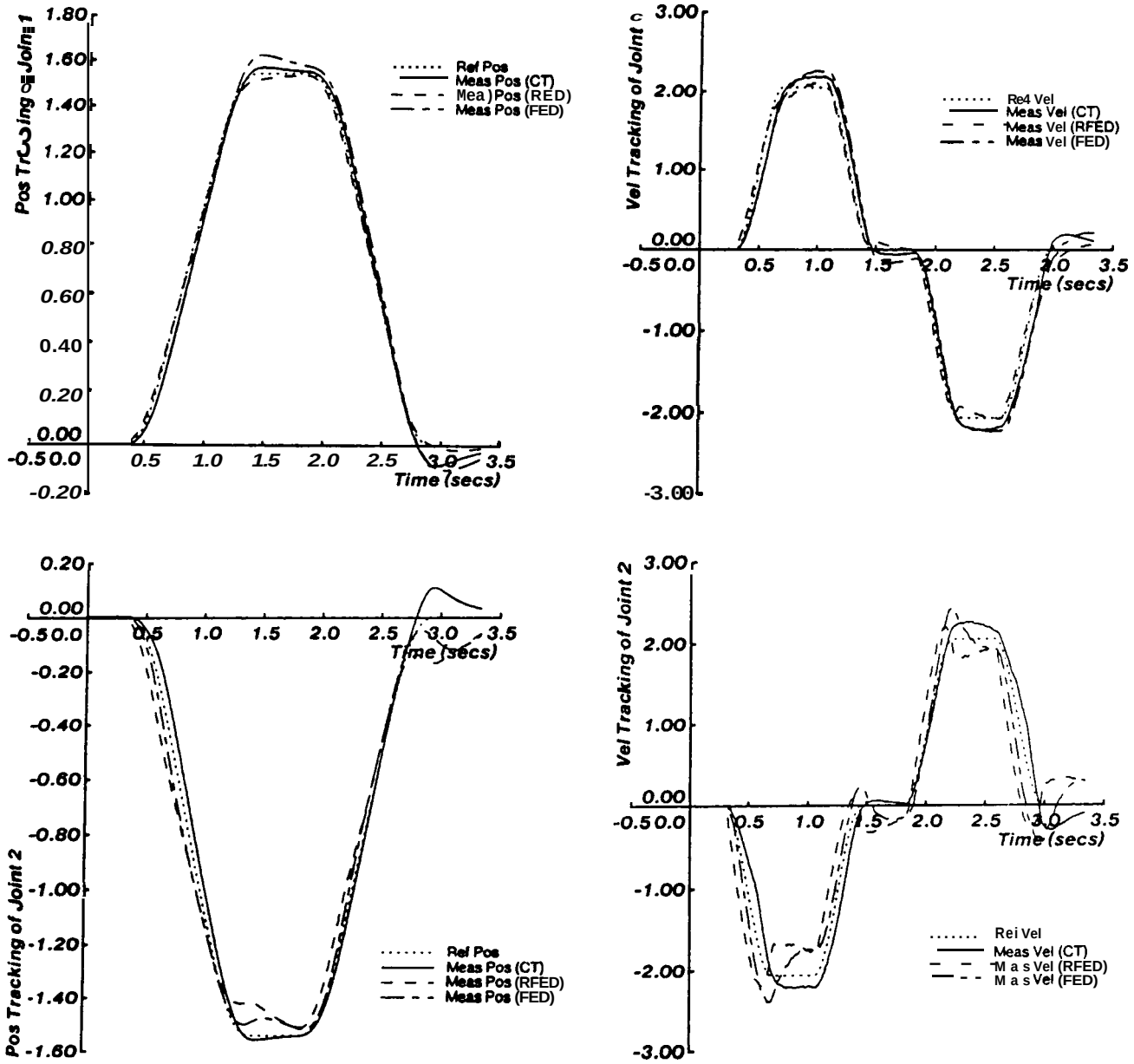

and Coriolis, and the gravity components of joints 1 through 3 is presented in Figs. **20–22.** First of all, we note that the applied torque for joint 1 has a profile similar to the desired acceleration of joint 1 except during the periods of constant speed **(0.75** to 1.0 **s** and **2.25** to **2.5 s)** in the trajectory. This suggests that the inertial torque $d_{11}\ddot{\theta}_1$ dominates along most part of the trajectory. This is further supported by the profile of the inertial torque component in Fig. **20.** The deviations observed in Fig. **20** are due to the Coriolis and the centrifugal components of the applied torque, which dominate during the period of constant velocity.

Fig. 11. Position tracking errors of joint 1.

Fig. 12. Position tracking errors of joint 2.

Fig. 13. Position tracking errors of joint 3.

Fig. 14. Velocity tracking errors of joint 1.

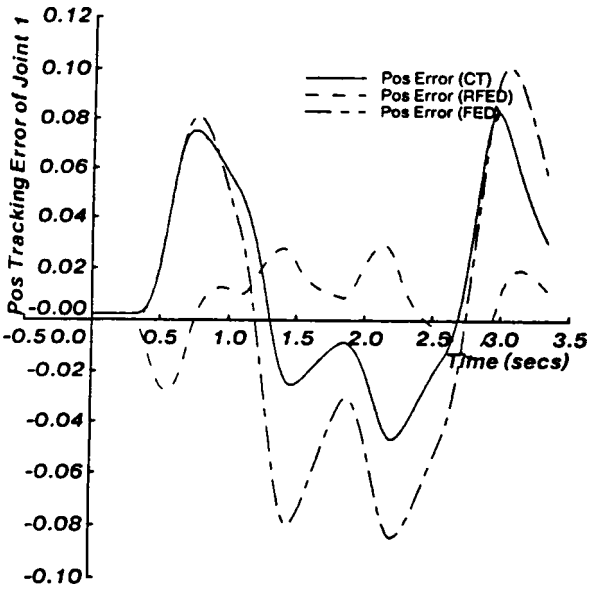

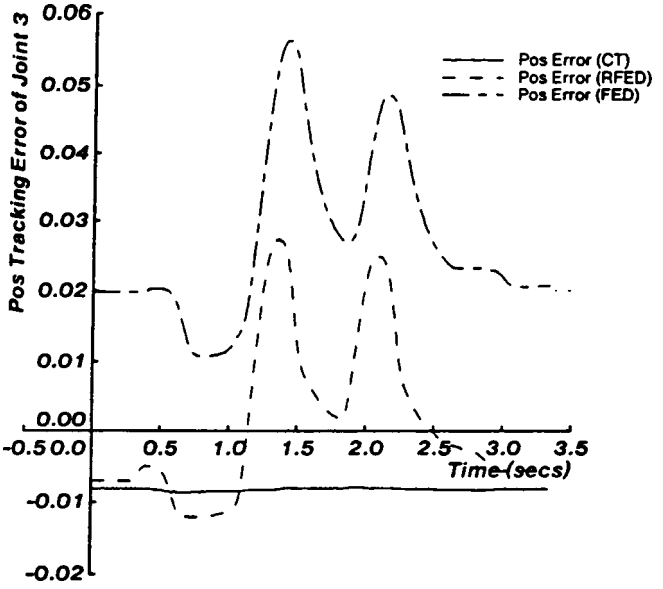

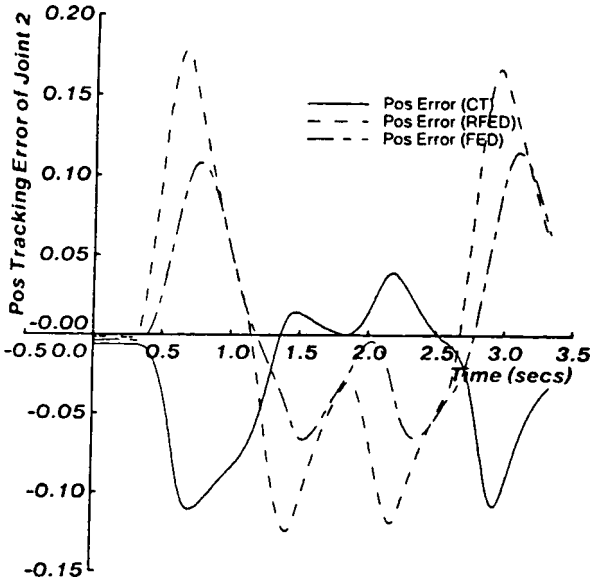

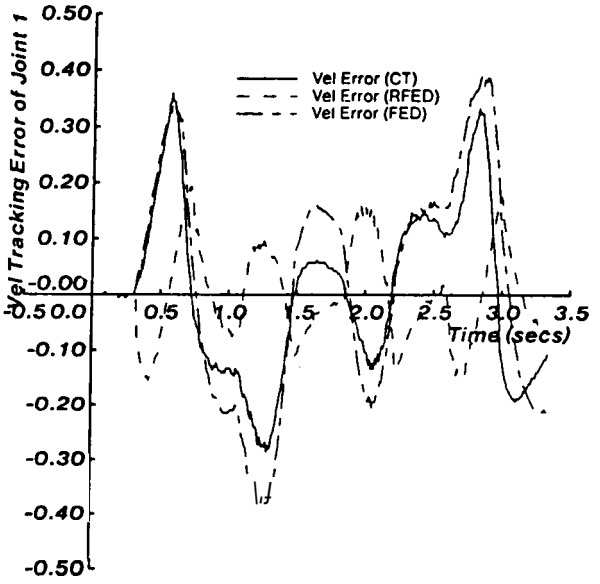

Next, in the case of joint 2 the inertial component of the applied torque curve in Fig. 21 is similar to the profile of the desired acceleration of joint 1 in Fig. 5. This implies that the applied torque of joint 2 is dominated by the inertial coupling term $d_{21}\ddot{\theta}_1$ along most of the trajectory. The term $h_{211}\dot{\theta}_1^2$ in Eq. (10) constitutes the centrifugal torque and is seen to dominate during periods of constant velocity.

Finally, in Fig. 22 the inertial component of the applied torque of joint 3 has a profile similar to the desired acceleration of joint 2, when the velocity dependent torques are negligible. This implies that the

Fig. 15. Velocity tracking errors of joint 2.

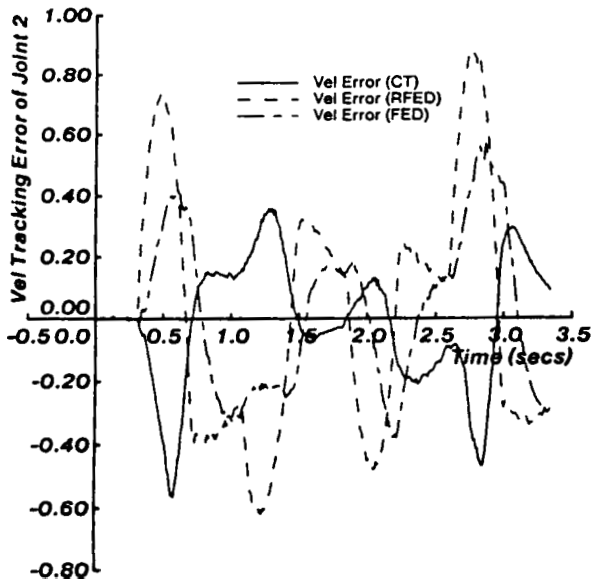

Fig. 16. Velocity tracking errors of joint 3.

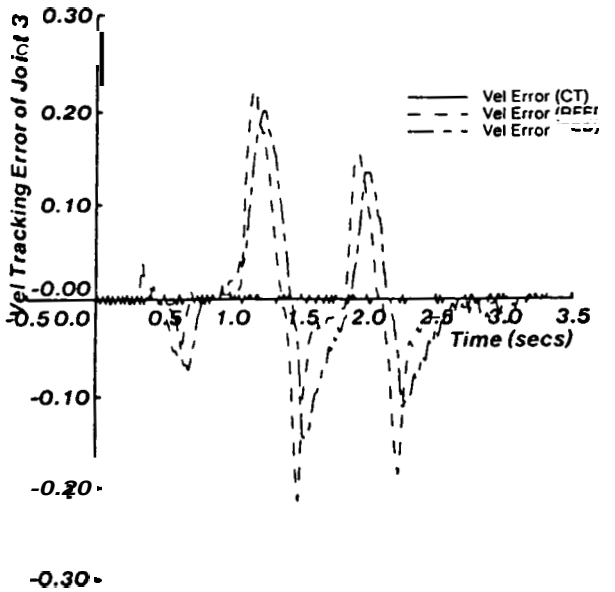

Fig. 17. Applied torque of joint 1.

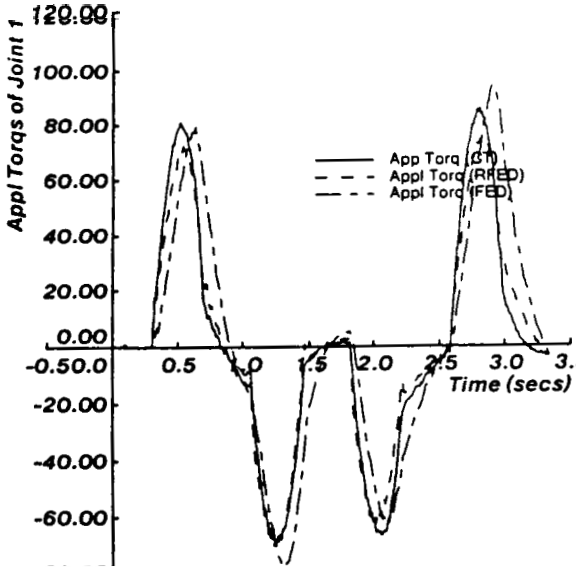

Fig. 18. Applied torque of joint 2.

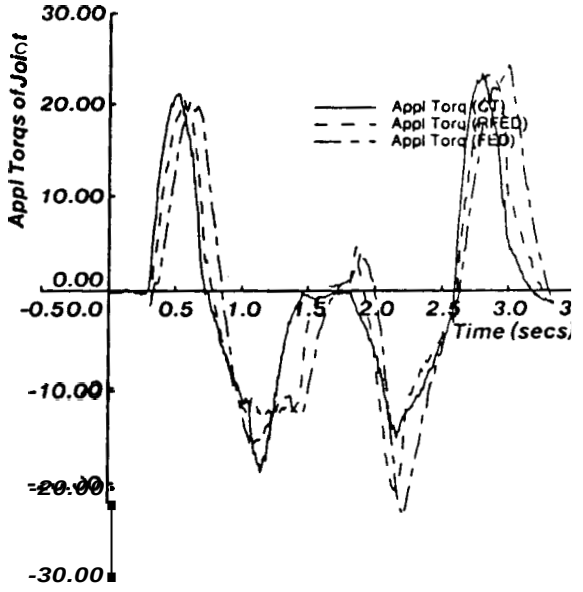

inertial coupling term $d_{32}\ddot{\theta}_2$ dominates along most part of the trajectory. The gravitational torque in Fig. 22 is due to the position errors and is negligible compared to the other torque components. It may be seen from Eq. (11) that the nonlinear velocity dependent torque consists of both the Coriolis and the centrifugal components arising out of the movement of links 1 and 2.

Fig. 19. Applied torque of joint 3.

Fig. 20. Torque components ofjoint 1 for CT.

Fig. 21. Torque components ofjoint 2for CT.

Fig. 22. Torque components ofjoint 3for CT.

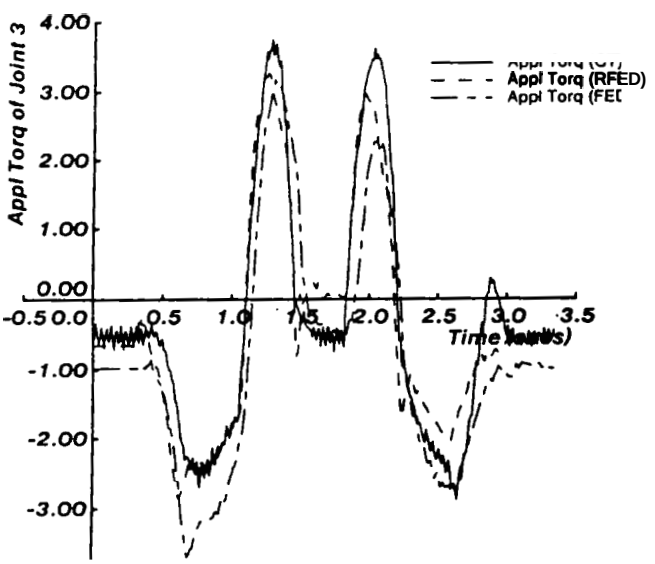

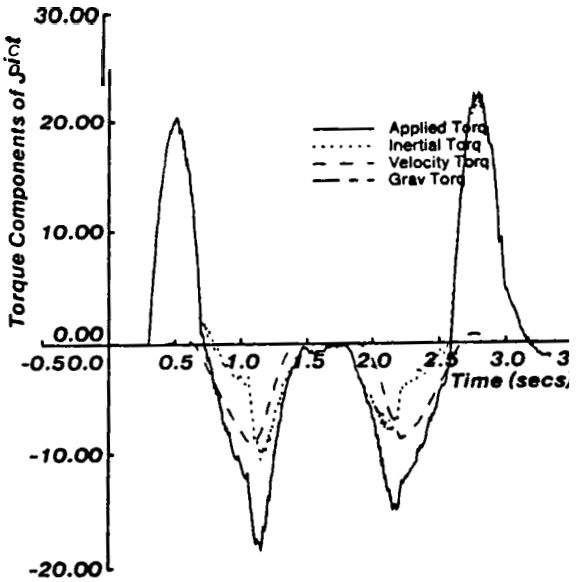

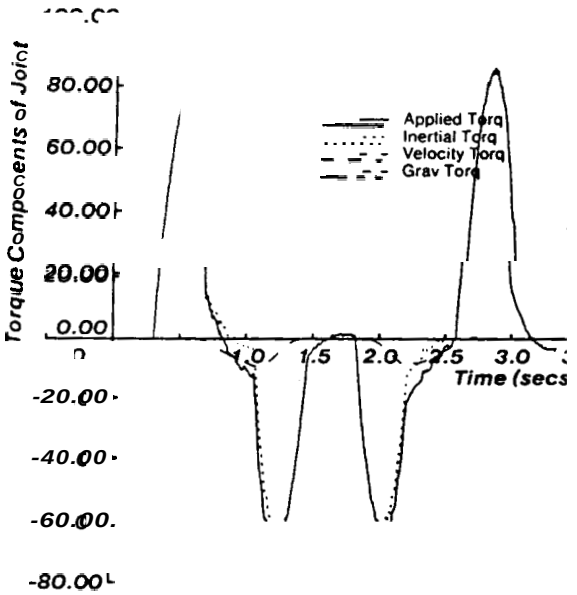

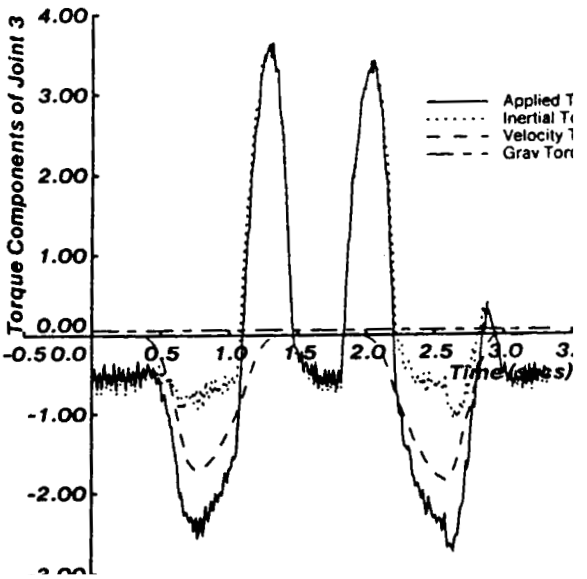

5. Conclusions

The aim of this paper has been twofold: to compare the performance of the feedforward dynamics compensation scheme with the computed-torque scheme, and to underscore the need for including the off-diagonal elements of the inertia matrix in the torque computation. The latter has been considered to be important particularly in the case of directdrive arms where the inertial coupling effects are accentuated due to lack of gears (Asada et al. 1982). It has been demon-

strated in our experiments and further supported by our analysis that it is possible for the off-diagonal terms to completely dominate the diagonal terms of the inertial matrix in the computation of the joint actuating torques. In such an event, neglecting the off-diagonal terms may lead to trajectory tracking errors. It must also be pointed out that if an *exact* model of the manipulator were available, then both the computed-torque and feedforward compensation scheme will give similar results. In such a circumstance, using the feedforward dynamics compensation may have some implementational advantages, because the feedforward torques could be computed off-line and added on-line to the torques computed by the independent joint controllers.

References

An, C. H., Atkeson, C. G., and Hollerbach, J. M. **1986** (San Francisco, California, April). Experimental determination of the effect of feedforward control on trajectory tracking errors. In Proc. ***IEEE Conf. on Robotics and Automation, ed.*** A. K. Bejczy. IEEE, pp. **55–60.**

Asada, H., Kanade, T., and Takeyama, I. **1982** (April). ***Control of a direct-drive arm.*** Technical Report CMU-RI-TR-82-4. The Robotics Institute, Carnegie Mellon University.

Bejczy, A. K. **1974** (February). ***Robot arm dynamics and control.*** Technical Memorandum **33-669.** Jet Propulsion Laboratory, Pasadena, Calif.

Brady, M., et **al. eds. 1982.** ***Robot motion: planning and control.*** Cambridge, Mass.: MIT **Press.**

Freund, E. **1982.** Fast nonlinear control with arbitrary pole placement for industrial **robots** and manipulators. ***Int. J. Robotics Res.*** **1(1):65–78.**

Gilbert, E. G., and Ha, I. J. **1984.** An approach to nonlinear feedback control and its application to robotics. ***IEEE Trans. Syst., Man Cybernet.*** **SMC-14(6):879–884.**

Horowitz, R., and Tomizuka, M. **1980** (Chicago, Illinois, November). An adaptive control scheme for mechanical manipulators—compensation of nonlinearity and decoupling control. ***Proc. ASME Winter Ann. Meeting.***

Kanade, T., Khosla, P. K., and Tanaka, N. **1984** (Las Vegas, Nevada, December). Real-time control of the CMU direct drive **arm II** using customized inverse dynamics. In ***Proc. 23rd IEEE ConJ on Decision and Control.*** ed. M. **P**. Polis. pp. **1345–1352.**

Khosla, P. K. **1986** (August). ***Real-time control and identification of direction-drive manipulators.*** Ph.D. Thesis, Department of Electrical and Computer Engineering, Carnegie Mellon University.

Khosla, P. K. **1987** (Raleigh, North Carolina, March). Choosing sampling rates for robot control. ***Proc. IEEE ConJ on Robotics and Automation.*** IEEE.

Khosla, P. K., and Kanade, T. **1985** (Florida, December). Parameter identification of robot dynamics. In ***Proc. 24th CDC, ed. G.*** F. Franklin. pp. **1754–1760.**

Khosla, P. K., and Kanade, T. **1986** (April). Real-time implementation and evaluation of model-based controls on CMU DD **arm II.** In ***IEEE Int. ConJ on Robotics and Automation. ed.*** A. K. Bejczy. IEEE.

Leahy, M. B., Valavanis, K. P., and Saridis, G. N. **1986** (San Francisco, California, April). The effects of dynamics models on robot control. ***Proc.*** IEEE *Conf.* ***on Robotics and Automation.*** IEEE.

Liegeois, Fournier and Aldon. **1980** (June). Model-reference control of high velocity **robots.** ***Proc. Joint ACC.*** **AACC.**

Neuman, C. P., and Khosla, P. K. **1985.** Identification of robot dynamics: an application of recursive estimation. In ***Advances in adaptive systems theory,*** ed. K. *S*. Narendra. New York: Plenum.

Raibert, M. H., and Horn, B. K. P. **1978.** Manipulator control using configuration space method. ***Industrial Robot*** **5:69–73.**

Schmitz, D., Khosla, P. K., and Kanade, T. **1985** (Tokyo, Japan, September). Development of CMU directdrive **arm II.** In ***Proc. 15th Int. Symp. on Industrial Robotics,*** ed. Yukio Hasegawa.

Seraji, H. **1986** (San Francisco, Calfiornia, April). Linear multivariable control of robot manipulators. ***Proc. IEEE Int. Conf. on Robotics and Automation.*** IEEE, pp. **565–571.**

Slotine, J-J. E. **1985.** The robust control of robot manipulators. ***Int. J. Robotics Res.*** **4(2):8***i* **-100.**

Tourassis, V. D. **1985** (June). ***Dynamic modeling and control of robotic manipulators.*** Ph.D. Thesis, Department of Electrical and Computer Engineering, Carnegie Mellon University.